Analysis of Microstrip Coupled Line Based Data-Signal and Energy Hybrid Receiver

N. M. Murad[a] and L. Rajaoarisoa[b] and S. Lalléchère[c] and G. Fontgalland[d] and B. Ravelo[e]

[a]Energy Lab (LE2P), Institut Universitaire de Technologie, Univ. La Réunion, 40, avenue de Soweto, BP 373 - 97455 Saint-Pierre cedex, France; [b]IMT Lille Douai, University of Lille, F-59000 Lille, France; [c] Université Clermont Auvergne (UCA), CNRS, SIGMA Clermont, Institut Pascal, F-63178 Aubière, France; [d] Federal University of Campina Grande, Applied Electromagnetic and Microwave Lab., Campina Grande/PB, 58429, Brazil; [e] Nanjing University of Information Science and Technology (NUIST), Nanjing, Jiangsu 210044, China

ARTICLE HISTORY
Compiled January 28, 2022

ABSTRACT
This paper develops an original circuit theory of energy and data transition. The modelling of innovative transition circuit combining signal and energy hybrid receiver (SEHR) is developed. The systemic topology of the SEHR is described with the different constituting blocks. The microstrip interconnect line design of the SEHR based on coupled line (CL) and a transmission line (TL) is modelled in equivalent circuit. The analytical modelling is performed with unfamiliar and arbitrary load values. The equivalent S-matrix model in function of the SEHR electrical parameters is established. The analysis of the S-matrix enables to predict the transmitted power and also the optimal condition of zero reflection in function of the terminal loads. The validity of the SEHR analytical model is verified with commercial tool simulations with a microstrip structure proof-of-concept. A configuration of electromagnetic (EM) environment operating at $2.45GHz$ with input power of about $0dBm$ is considered. The prediction of detected average energy and transmitted data-signal voltage amplitude in function of SEHR electrical and geometrical parameters is discussed.

KEYWORDS
Energy and data; S-matrix; Analytical modelling; Circuit theory; Microstrip circuit; Parametric analysis; Signal and energy hybrid receiver (SEHR); Topology; Transition structure

1. Introduction

Today, a general survey reports that behind the massive deployment of tens of billions of connected objected, the wireless sensor networks (WSNs) are expected as the ultimate technological solution to ensure the data transmission [1,2]. The energy-efficiency (EE) is one of the principal criteria for the wireless sensor network (WSN) performances [1,14].

The EE of neighboured mobile devices was investigated [3,4]. It was found that the WSN EE depends on the clustering protocols [1,5,6] and the data coding techniques

CONTACT B. Ravelo. Email: blaise.ravelo@yahoo.fr

such as OOK [7]. To improve the EE performance, certain internet protocols (IPs) intended to operate with energy harvesting (EH) were proposed [6]. In addition to the protocols, the other communication layers as the physical systems play also a major role in the EE performance [7–9]. Subsequently, intensive technological researches have been realized to design power sensitive and best Size Weight and Performance (SWAP) transceiver CMOS integrated circuits (ICs) [8,9]. More importantly, systemic solutions based on power control optimization were also introduced [10–12]. The ideal solution of power optimization conducted to the deployment of electromagnetic (EM) EH implementation [1,11–14]. A study on the impact of EH on the WSN security was carried out in [11]. An energy prediction algorithm was developed in function of EH parameters in [12]. And a more synergic study on the system and protocol of wake-up radio circuit for the EE optimization was reported in [13]. Besides, the investigation on EH circuits raises a curious question on the performance related to the data collection [14]. The circuit-level investigation on the data signal and EE depends inherently to the power control and measurement approaches [10,15]. The wireless and radio frequency (RF) power measurement implies the development of power sensor devices [16,17]. However, the optimization of WSN EE and data collection depending on the measurement technique, for example with GaAs [16] and MEMS [17] MMIC sensors are particularly fastidious and too expensive. Therefore, research must go on the design and analysis of simpler passive circuit susceptible to vehiculate data signal and energy to feed WSNs.

In the present study, we would be more original to develop a hybrid receiver system capable to collect the data signal and EM energy simultaneously. We expect an original solution based on the basic well-known concept of crosstalk or EM coupling circuit, for example, implemented with electrical signal interconnects transmission lines (TLs) [18–23]. The crosstalk effects are classified as undesirable EM compatibility (EMC) issues in the electrical interconnects confined printed circuit boards (PCBs) [18]. The crosstalk constitutes also a widely deployed topology of tremendous RF and microwave circuits as coupler, filter, and unfamiliar electronic functions as negative group delay (NGD) concepts [19–23]. The coupled line (CL) based innovative signal-energy hybrid receiver (SEHR) proposed in the present paper is prominent on the possibility of various parameter analytical modelling and prediction.

First, the received wireless RF energy and power repartition can be investigated with the S-parameter approach [24–26]. Moreover, it allows also to predict the signal and energy propagation delay [27–31] through the TL SEHR transition. The presentation of the proposed SEHR is performed in the following three sections: Section 2 is focused on the topological description of the SEHR circuit. The topology of the SEHR is fundamentally based on the CL connected to unfamiliar load impedances. The equivalent S-matrix will be established from the impedance matrix or Z-matrix operation as investigated in [32]. The general S-matrix of the SEHR will be expressed in function of elementary constituting element parameters. Section 3 develops an application study based on parametric simulations of S-parameters representing the power repartition in function of the SEHR loads. Section 4 is the conclusion.

2. Analytical description of the SEHR implemented with CLs

The present section introduces the analytical theory of the SEHR system. The SEHR system will be described. The 3-D views illustrating the technological implementation will be developed. The equivalent circuit will serve for the theoretical analysis and

S-matrix modelling.

2.1. General Description of the SEHR System

The present theory is constructed under the context of wireless communication. The information is transmitted via harmonic EM wave having a frequency, f_0, propagating in an open space environment. The EM energy is converted into an electric voltage source with an ideal harvester. The proposed SEHR is dedicated to being connected in downstream of the harvester. However, few studies are available in the literature about the analytical investigation and design of SEHR. The following study will give answers to this curious challenge.

Figure 1(a) illustrates the synoptic diagram of the proposed SEHR. It is mainly constituted of five different parts. The synoptic diagram input port ① is constituted by the receiver antenna, which enables to convert the EM wave from open space environment. The input connected to port ① represents the EM wave (data + energy) information available in the environment. Between ports ① and ②, we have a transition block and that is connected the energy recovery load. Between ports ① and ③, the transition block is intended to drive the data signal into the last block representing the received signal load. Acting as a three-port structure, an equivalent block diagram of the SEHR is proposed in Figure 1(b). The input can be represented by a harmonic voltage source, with real positive amplitude, U_0, denoted:

$$U(j\omega) = U_0 \exp(j\omega T_0) \tag{1}$$

with the variable angular frequency $\omega = \omega_0 = 2\pi f_0$, and time variable, T_0. The internal impedance of this source is represented by a resistor, R_1. The two-output ports, ② and ③, are constituted by the received signal and the delivered energy respectively. The main block ensures the transmission of the signal containing data and energy to the receiver. The terminals of the data and energy transition blocks are supposed connected to resistive loads, R_2 and R_3. Before the analytical modelling, the equivalent circuit to implement this SEHR topology will be described in the next subsection.

The following part of this analytical theory is dedicated to the elaboration of the SEHR black box and, especially, its efficiency in function of loads R_1, R_2 and R_3.

2.2. Equivalent Circuit of the SEHR

To preserve the energy-efficiency, the SEHR system is implemented with a completely passive microstrip circuit. Figure 2 highlights the profile view constituted by metallization conductor line, ground plane and dielectric substrate. The main geometrical parameters of the microstrip line are the conductor line width, w, thickness, t, and substrate height, h.

The main originality of the SEHR circuit is its structural implementation with a three-port configuration of microstrip CL, which delivers the signal from source to two different loads, R_2 and R_3. Figure 3(a) depicts the 3-D design of the CL based SEHR. It is essentially composed of two lossless TLs. The first one connected between ports ① and ②, and the other one is connected between ports ③ and an open-ended port. The two microstrip TLs are defined with geometrical parameters, width-length (w, d) and $(w_d, d + d_d)$, respectively. The physical interspace between the two TLs is

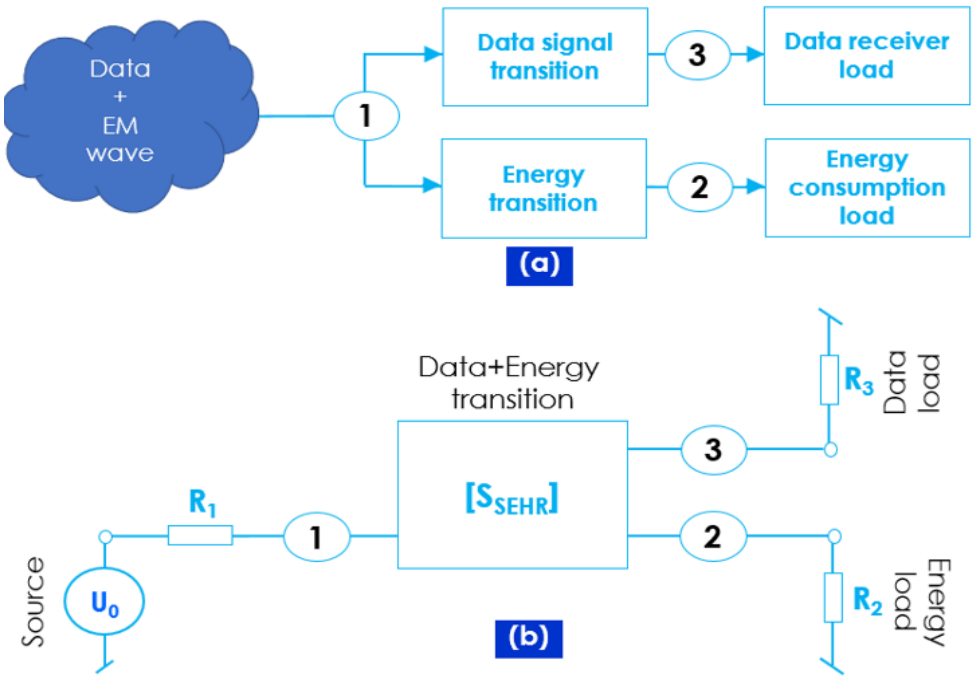

Figure 1.: Graphical idea of the SEHR system: (a) Synoptic diagram (b) Block diagram with the input and output access resistive loads

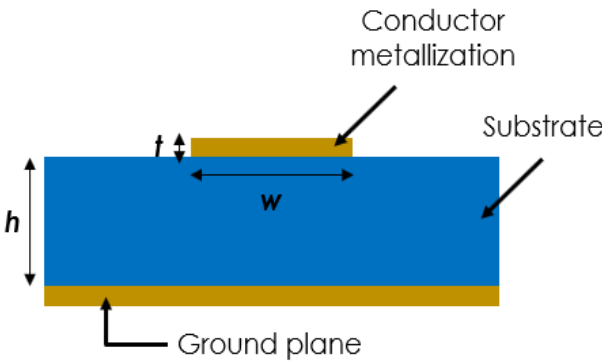

Figure 2.: Profile view of microstrip line

denoted by s. To perform the theoretical study of this SEHR system, we propose the equivalent circuit depicted in Figure 3(b). The source is equivalent to voltage-internal output impedance (U_0, R_1).

The TL connected to the signal data reception load can be realized by splitting TLs into two pieces of TLs with physical lengths, d and d_d. The main block can be represented by a CL, noted, $CL(Z, k, d)$, with characteristic impedance, Z, coupling coefficient, k, physical length, d, and the two-port TL, noted, $TL(Z_D, d_d)$, with characteristic impedance, Z_D, and physical length d_d.

The next paragraphs define the characteristics of SEHR circuit components.

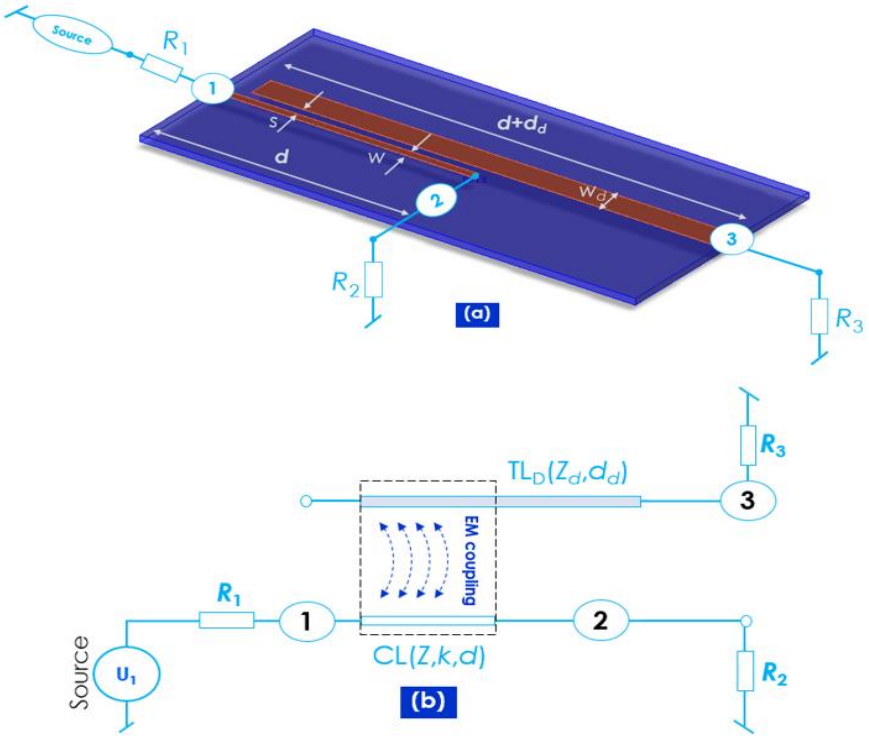

Figure 3.: Configuration of the SEHR: (a) Microstrip circuit implementation (b) Three-port equivalent circuit

2.3. Analytical Investigation on SEHR Equivalent Z-Matrix

The SEHR circuit analysis in the present paper will be elaborated with Z-matrix approach. The analytical investigation of previously introduced system is presented in the next paragraphs.

2.3.1. Description of SEHR Constituting Element Electrical Parameters

In addition to the resistive loads, the main electrical elements of the SEHR can be extracted from the physical parameters from Hammerstad-Jensen microstrip TL and CL models [33,34]. The main parameters are the characteristic impedances Z and Z_D of the TLs connected to external port ② and port ③. These characteristic impedances determined from Figure 4(a) represents the equivalent circuit with the splitted TLs and the CL. By taking the TL wave speed, v, and the variable angular frequency, ω, the propagation constant of the signal travelling through these TLs can be expressed as follows:

$$\gamma(j\omega) = \exp(-j\omega\tau) \tag{2}$$

$$\gamma_D(j\omega) = \exp(-j\omega\tau_D) \tag{3}$$

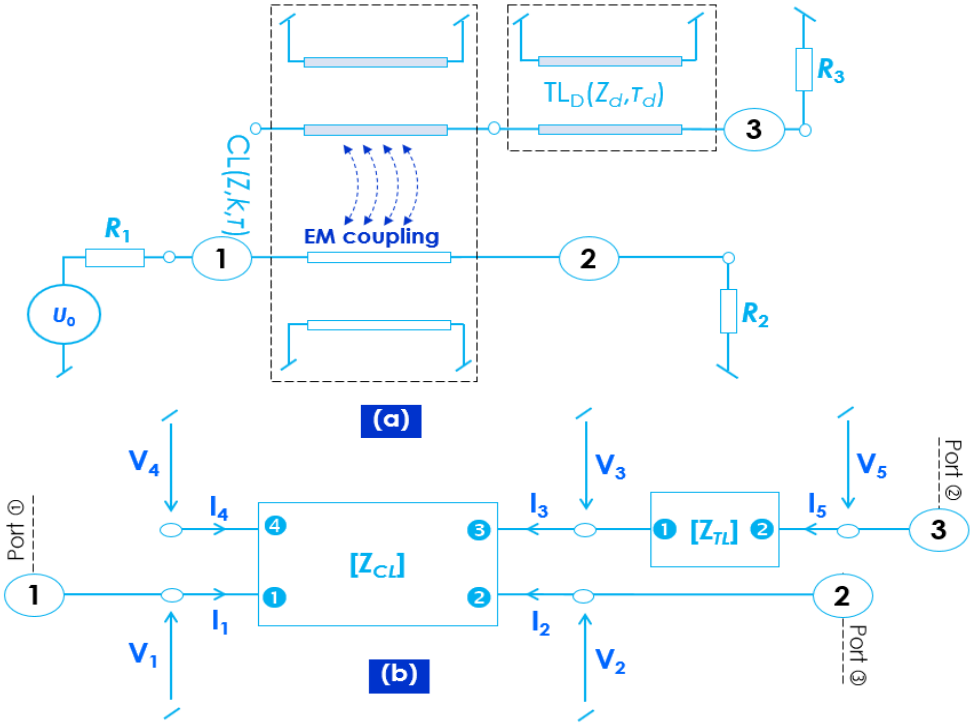

Figure 4.: Equivalent diagram of the circuit introduced in Figure 3(b): (a) TL-based equivalent circuit (b) Equivalent block diagram

where the propagation delays:

$$\begin{cases} \tau = & d/v \\ \tau_D = & d_d/v. \end{cases} \tag{4}$$

2.3.2. Description of Constituting Elementary Z-Matrix

Similar to the microstrip structure analysis proposed for some microwave circuits [22-23,30], the black boxes equivalent to the constituting elements must be defined. Substantially, let consider the impedance or Z-matrix [32] block circuit of the system diagram depicted in Figure 4(b). Accordingly, we remind that:

- The equivalent 2-D Z-matrix of the two-port TL, $TL_D(Z_D, \tau_D)$ with internal ports ① and ②, is written as:

$$\left[Z_{TL_D}\right] = jZ_D \begin{bmatrix} \frac{1}{tan(\omega\tau_D)} & \frac{1}{sin(\omega\tau_D)} \\ \frac{1}{sin(\omega\tau_D)} & \frac{1}{tan(\omega\tau_D)} \end{bmatrix}. \tag{5}$$

- The CL is assumed defined by the characteristic impedance, Z, and coupling coefficient, k. Therefore, the even- and odd-mode characteristic impedances are

given by:

$$\begin{cases} Z_e = & Z\sqrt{\frac{1+k}{1-k}} \\ Z_o = & Z\sqrt{\frac{1-k}{1+k}} \end{cases} . \tag{6}$$

Following internal and secondary ports ❶, ❷, ❸, and ❹, the equivalent Z-matrix of the CL must be with 4-dimension given by:

$$\left[Z_{CL}\right] = \begin{bmatrix} Z_{11} & \dots & Z_{14} \\ \vdots & \ddots & \vdots \\ Z_{41} & \dots & Z_{44} \end{bmatrix} \tag{7}$$

with:

$$\begin{cases} Z_{11} = & Z_{22} = Z_{33} = Z_{44} = \frac{Z_e+Z_o}{2jtan(\omega t)} \\ Z_{12} = & Z_{21} = Z_{34} = Z_{43} = \frac{Z_e-Z_o}{2jsin(\omega t)} \\ Z_{13} = & Z_{31} = Z_{24} = Z_{42} = \frac{Z_e-Z_o}{2jsin(\omega t)} \\ Z_{14} = & Z_{41} = Z_{23} = Z_{32} = \frac{Z_e+Z_o}{2jsin(\omega t)} \end{cases} . \tag{8}$$

2.3.3. Z-Matrix Model of the SEHR

According to the circuit and system theory, acting as a three-port topology, the Z-matrix equivalent model of the SEHR can be expressed as:

$$\left[Z_{SEHR}\right] = \begin{bmatrix} Z_{S11} & Z_{S12} & Z_{S13} \\ Z_{S21} & Z_{S22} & Z_{S23} \\ Z_{S31} & Z_{S32} & Z_{S33} \end{bmatrix} \tag{9}$$

with

$$Z_{S11} = Z_{S12} = Z_{S21} = Z_{S22} = \frac{-j\{X_s^2[2X_tZ(Z_e+Z_o)+(Z_e+Z_o)^2Y_t]+X_t^2Y_t(Z_o-Z_e)^2\}}{2X_s^2X_t[2X_tZ+Y_t(Z_e+Z_o)]}$$

$$Z_{S13} = Z_{S23} = \frac{jZX_tY_t(Z_o-Z_e)}{X_sY_s[2X_tZ+Y_t(Z_e+Z_o)]}$$

$$Z_{S31} = Z_{S32} = \frac{jZY_t(Z_o-Z_e)}{X_s[2X_tZ+Y_t(Z_e+Z_o)]}$$

$$Z_{S33} = \frac{-jZY_t(Z_e+Z_o)}{Y_s[2ZX_t+Y_t(Z_e+Z_o)]}$$

and

$$\begin{cases} X_s = & sin(\omega\tau) \\ X_t = & tan(\omega\tau) \\ Y_s = & sin(\omega\tau_D) \\ Y_t = & tan(\omega\tau_D) \end{cases}.$$

The mechanism of determination of the nine elements constituting this matrix can be methodologically determined following the configuration of access voltages and access currents of the electrical block diagram presented in Figure 4(b). For starting, the generalized Ohm's law applied to each element, TL and CL of the SEHR can be expressed as, respectively:

$$\begin{bmatrix} V_1 \\ V_2 \\ V_3 \\ V_4 \end{bmatrix} = \begin{bmatrix} Z_{CL} \end{bmatrix} \begin{bmatrix} I_1 \\ I_2 \\ I_3 \\ I_4 \end{bmatrix} \tag{10}$$

$$\begin{bmatrix} V_3 \\ V_5 \end{bmatrix} = \begin{bmatrix} Z_{TL} \end{bmatrix} \begin{bmatrix} -I_3 \\ I_5 \end{bmatrix}. \tag{11}$$

The mathematical handling of these matrices follow the electrical configuration shown in Figure 4(b), where the Z-matrix of equation (9) can be expressed in function of the SEHR electrical parameters defined in the previous paragraphs. As the fourth access port of CL is open-ended, we have current $I_4 = 0$. Substituting the expressions of voltages, V_4 and V_5, and current, I_5, the following matrix relationship to determine the nine elements of the matrix, $[Z_{SEHR}]$, can be established:

$$\begin{bmatrix} V_1 \\ V_2 \\ V_5 \end{bmatrix} = \begin{bmatrix} Z_{SEHR} \end{bmatrix} \begin{bmatrix} I_1 \\ I_2 \\ I_5 \end{bmatrix}. \tag{12}$$

It is noteworthy that the present study is focused on the case of mono-frequency analysis with $\omega = \omega_0 = 2\pi f_0$. The choice of the TL and CL electrical parameters is made to have a quarter wavelength and multiple of the full wavelength, respectively:

$$\tau = \frac{1}{4f_0} \tag{13}$$

and

$$\tau_D(n) = \frac{n}{f_0} \tag{14}$$

where the positive integer, n, can be chosen in function of the synchronization between the data and energy detections by the terminal loads.

2.4. Analytical Investigation on SEHR Equivalent S-Matrix

The present S-matrix analysis of the SEHR system is conducted from the Z-matrix established in the previous subsection.

2.4.1. S-Matrix Model of the SEHR

We recall that acting as a three-port topology, the SEHR S-matrix model can be expressed as:

$$\left[S_{SEHR}(j\omega)\right] = \begin{bmatrix} S_{11}(j\omega) & S_{12}(j\omega) & S_{13}(j\omega) \\ S_{21}(j\omega) & S_{22}(j\omega) & S_{23}(j\omega) \\ S_{31}(j\omega) & S_{32}(j\omega) & S_{33}(j\omega) \end{bmatrix} \tag{15}$$

In difference to the studies available in the literature [22-26], the present S-matrix modelling is established under the hypothesis that the terminal reference loads are represented by the 3-D matrix:

$$\left[Z_{ref}\right] = \begin{bmatrix} R_1 & 0 & 0 \\ 0 & R_2 & 0 \\ 0 & 0 & R_3 \end{bmatrix} \tag{16}$$

As a matter of fact, the SEHR S-matrix can be extracted from Z-to-S matrix transform:

$$\left[S_{SEHR}(j\omega)\right] = \begin{cases} (\left[Z_{SEHR}(j\omega)\right] - \left[Z_{ref}\right])\times \\ (\left[Z_{SEHR}(j\omega)\right] + \left[Z_{ref}\right]^{-1}) \end{cases} \tag{17}$$

2.4.2. S-Matrix Model Versus the SEHR Electrical Parameters

Let us denote P_1, P_2, and P_3, the input power injected at port ① and output powers received at port ② and port ③. For the sake of the analytical simplification, in the present study, we focus our attention to the S-parameter elements corresponding to:

- the reflected signals at the three ports, ①, ②, and ③, quantified by S_{11}, S_{22}, and S_{33},
- and the transmitted signals from port ① to port ② quantified by S_{21} and from port ① to port ③ quantified by S_{31}, given by:

$$|S_{21}| = \sqrt{\frac{P_2}{P_1}} \;\Rightarrow\; P_2 = S_{21}P_1 \tag{18}$$

$$|S_{31}| = \sqrt{\frac{P_3}{P_1}} \;\Rightarrow\; P_3 = S_{31}P_1. \tag{19}$$

It can be derived from matrix relation (17) that we have the reflection coefficients:

$$S_{11} = \frac{(R_2 - R_1)(Z_e^2 + Z_o^2) - 2Z_eZ_o(R_1 + R_2) + 4R_1R_2R_3}{D} \tag{20}$$

$$S_{22} = \frac{(R_1 - R_2)(Z_e^2 + Z_o^2) - 2Z_eZ_o(R_1 + R_2) + 4R_1R_2R_3}{D} \tag{21}$$

$$S_{33} = \frac{(R_2 + R_1)(Z_e^2 + Z_o^2) - 2Z_eZ_o(R_1 - R_2) + 4R_1R_2R_3}{D} \tag{22}$$

$$S_{21} = \frac{2\sqrt{R_1R_2}(Z_e^2 - Z_o^2)}{D} \tag{23}$$

$$S_{31} = \frac{4jR_3\sqrt{R_1R_2}(Z_e - Z_o)}{D} \tag{24}$$

with:

$$D = (R_1 + R_2)(Z_e^2 + Z_o^2) + 2Z_eZ_o(R_1 - R_2) - 4R_1R_2R_3. \tag{25}$$

We can remark that the ratio between the power transmitted from port ① ② and ① ③ are given by:

$$\alpha = \left|\frac{S_{21}}{S_{31}}\right| = \frac{Z_e + Z_o}{2\sqrt{R_2R_3}}. \tag{26}$$

2.4.3. Input Perfectly Matched SEHR Electrical Parameters

A perfectly matched SEHR circuit is realized when $S_{11} = 0$, which corresponds to the situation that all the input power, from port ①, are completely transmitted to output ports ② and ③. By taking into account of equation (20), we have:

$$R_3 = \frac{2Z_eZ_o(R_1 + R_2) + (R_1 - R_2)(Z_e^2 + Z_o^2)}{4R_1R_2}. \tag{27}$$

In the case where R_1 is given, the existence condition of this load is:

$$R_2 < R_{2max} = R_1\frac{(Z_e + Z_o)^2}{(Z_e - Z_o)^2}, \tag{28}$$

knowing R_2, it is equivalent to:

$$R_1 > R_{1min} = R_2\frac{(Z_e - Z_o)^2}{(Z_e + Z_o)^2}. \tag{29}$$

In this case, the transmission coefficients established in equations (23) and (24) become; respectively

$$|S_{21}(S_{11} = 0)| = \left|\frac{(Z_e + Z_o)}{(Z_e - Z_o)}\right|\sqrt{\frac{R_1}{R_2}} \tag{30}$$

$$|S_{31}(S_{11}=0)| = \frac{\sqrt{(R_1-R_2)(Z_e^2+Z_o^2)+2Z_eZ_o(R_1+R_2)}}{\sqrt{2R_2}(Z_e-Z_o)} \tag{31}$$

2.4.4. Synthesis Equations of (R_1, R_2) Given (P_2/P_1, P_3/P_1)

Under the hypothesis of perfectly matched SEHR with R_3 expressed in (27), we can synthesis resistors R_1 and R_2. Given the desired power ratio between the powers transmitted at port $m = 2, 3$ and injected at port ①; we can write

$$\alpha_{(m=2,3)} = \frac{P_m}{P_1}. \tag{32}$$

In this case, we can determine resistors R_1 or R_2, by inverting equations (30), and we have:

$$R_1 = \alpha_2 R_2 \left|\frac{Z_e - Z_o}{Z_e + Z_o}\right|^2. \tag{33}$$

By inverting equation (32), we have:

$$\alpha_3 R_2 (Z_e - Z_o)^2 = (R_1 - R_2)(Z_e^2 + Z_o^2) + 2Z_eZ_o(R_1 + R_2) \tag{34}$$

From (34), after simplification

$$R_2 = \frac{R_1[(Z_e + Z_o)^2]}{(1+\alpha_3)(Z_e - Z_o)^2}. \tag{35}$$

As numerical application of the developed theory, the parametric simulations in function of the SEHR loads will be discussed in the next section.

3. Application study of the SEHR load and parameter influences

After the proof-of-concept (POC) description, the simulated results of power repartition will be introduced in the following subsections. It is noteworthy that the present study is essentially carried out within the schematic environment of electronic and RF circuit design and simulator ADS® from Keysight Technologies®.

3.1. POC Description, and Mono-frequency Average Energy and Transmitted Data-Signal Amplitude

A microstrip POC design will be described in the following paragraph.

3.1.1. ADS® Design of SEHR POC

Figure 5 represents the ADS® design of the simulated SEHR POC. It is composed of microstrip models of TL and CL implemented in microstrip technology defined in [33–35]. To perform the S-parameter simulations, we have to consider the terminals, $Term(m)$, representing the source and loads at port $m = 1, 2, 3$. The associated internal resistor of $Term(m)$ is denoted by R_m. A Rogers substrate with striped Cu

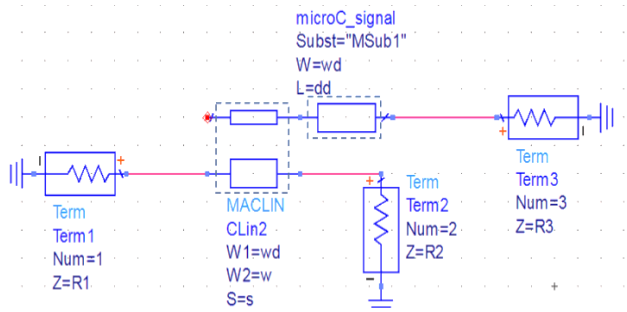

Figure 5.: Illustrative design of the simulated SEHR

metallization was considered for this POC. Table 1 represents the physical parameters w, w_d, and s, of the substrate and the electrical parameters R_1, R_2, and R_3 of the TL and CL elements.

Table 1.: Microstrip circuit parameters of the SEHR POC

Constituting element	Designation	Parameters	Values
Substrate	Dielectric substrate thickness	h	$1.27mm$
	Relative permittivity	ε_r	10.2
	Metallization thickness	t	$35\mu m$
	Loss tangent	$tan(\delta)$	0.0027
	Metallization conductivity	σ	$58MS/m$
Interconnect lines [35]	CL	w	$3mm$
		d	$10.8mm$
		s	$2mm$
		Z_e	30.6Ω
		Z_0	26.4Ω
		τ	$102ps$
	TL_D	w_d	$1mm$
		d_d	$44.3mm$
		Z_d	52Ω
		τ_d	$408ps$
Reference loads	Port ①	R_1	10Ω
	Port ②	R_2	100Ω
	Port ③	R_3	$1M\Omega$

3.1.2. Computed Average Energy and Data-Signal Amplitude

The S-parameter analysis of this SEHR was performed at the mono-frequency, $f_0 = 2.456GHz$. The input average power is assumed equal to $P1 = 0dBm$. In addition to

the average power, the average energy per period received at port ② is given by:

$$E_2 = \frac{P_2}{f_0}. \tag{36}$$

The amplitude of output signal voltage detected at port ③ can be calculated with:

$$V_3 = S_{31}\sqrt{R_3 P_1}. \tag{37}$$

The average power, energy and reflection coefficients of SEHR based on the parameter indicated in Table 1 are given in Table 2.

Table 2.: SEHR POC coefficient values

Description	Parameters	Values
Power	P_2	$-0.045dBm$
	P_3	$-58.005dBm$
Reflection coefficient	S_{11}	$-20.07dB$
	S_{22}	$-20.06dB$
	S_{33}	$-32\mu dB$
Energy period	E_2	$0.406pJ$
Voltage amplitude	V_3	$6.3V$

The parametric analysis of SEHR main electrical and geometrical parameter will also be explored in the following paragraphs.

3.2. Parametric Analysis with Respect to the SEHR Loads

The present parametric analyses were performed with respect to the SEHR circuit electrical and geometrical parameters, R_1, R_2, R_3, s, w and w_d. The simulation analyses correspond to the computed result of reflection parameters, transmitted average power, detected average energy and transmitted data-signal amplitude. The results were simulated with ADS® single frequency, $f_0 = 2.45GHz$, and sweeping linearly the previously indicated parameters.

3.2.1. Parametric Analysis with Respect to R_1

The present parametric analysis is performed for the resistor, R_1 varied from 10Ω to 20Ω by fixing the other parameters as shown in Table 1.

The generated results are plotted in Figure 6. The reflection coefficients, S_{11} and S_{22} reach their minimal value $S_{11min} = -23.2dB$ at R_{1min} of about 8.6Ω as seen in Figure 6(a). The output powers detected at ports ② and ③, are shown in Figure 6(b). At the same value of R_1, we can emphasize from Figure 6(c) that the maximal value of average energy per period transmitted at port ②, $E_{2max} = 0.405nJ$. As displayed in Figure 6(d), the amplitude of voltage, V_3 presents its maximal value of about $1.26V$.

3.2.2. Parametric Analysis with Respect to R_2

The present case of parametric analysis was carried out with respect to the resistor, R_2 varied from 50Ω to 200Ω, by fixing the other parameters of the SEHR circuit as

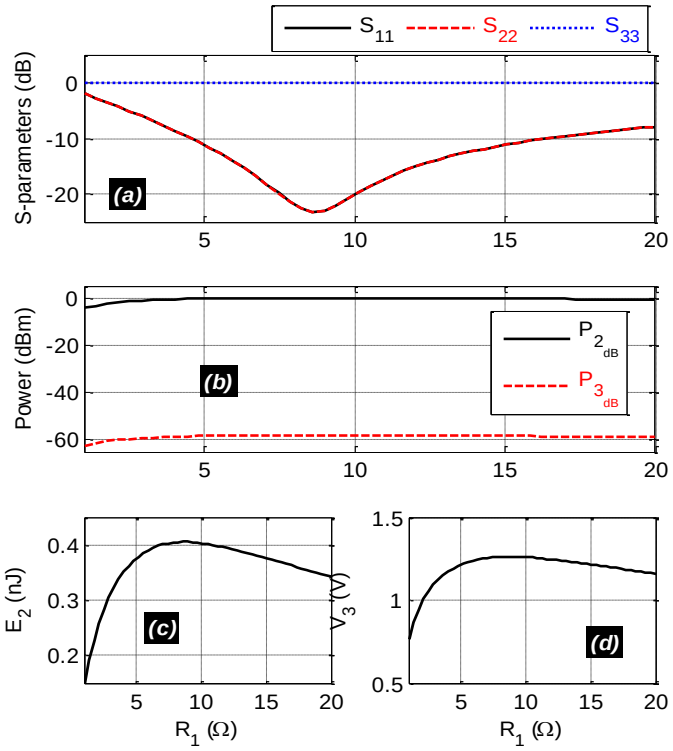

Figure 6.: Parametric analysis results with respect to R_1 (a) Reflection coefficients (b) Power (c) Energy per period, E_2 (d) Amplitude of voltage, V_3

shown in Table 1.

The simulated results are plotted in Figure 7. It can be seen in Figure 7(a) that the reflection coefficients present behaviors similar to the previous analysis. The reflection coefficients, S_{11} and S_{22} reach their minimal value $S_{11min} = -24.8dB$ at R_{2min} of about 85.5Ω as seen in Figure 7(a). The output powers detected at ports ② and ③ with respect to the variation of R_2, are shown in Figure 7(b). At the other optimal value of $R_{2opt} = 77.6\Omega$, we can emphasize from Figure 7(c) that the maximal value of energy per period transmitted at port ②, $E_{2max} = 0.405nJ$. As displayed in Figure 6(d), the amplitude of voltage, V_3 increases with R_2, from $0.94V$ to $1.594V$. In conclusion, a compromise has to be made on the choice of R_2, for the practical cases.

3.2.3. Parametric Analysis with Respect to R_3

This third paragraph of parametric analysis corresponds to the variation of the resistor R_3 varied from $0.1M\Omega$ to $10M\Omega$, by fixing the other parameters of the SEHR circuit as shown in Table 1.

The reflection coefficients with respect to R_3, are plotted in Figure 8(a). The two output powers are displayed in Figure 8(b). We can underline that in contrast to the two previous paragraphs, the considered resistor load does not affect significantly the S-parameters. The average energy E_2 is rather constant, of about $0.4nJ$. Nevertheless, the output voltage V_3 delivered from the port is decreasing from $3.98V$ to $0.39V$ in the considered range of R_3. This result can be exploited in the future in the function of the load as mixed circuit technology for the adequate level of voltage for signal

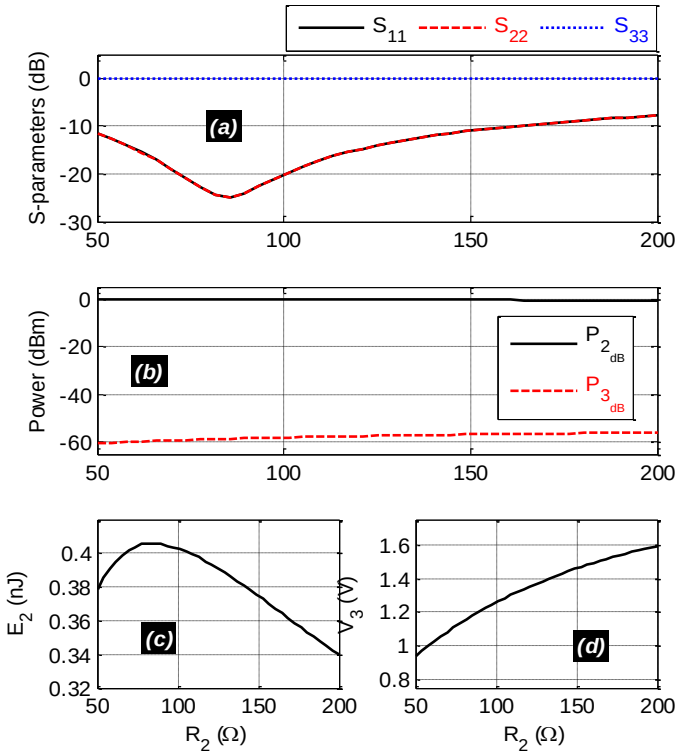

Figure 7.: Parametric analysis results with respect to R_2 (a) Reflection coefficients (b) Power (c) Energy per period, E_2 (d) Amplitude of voltage, V_3

detection and decoding.

3.2.4. Parametric Analysis with Respect to s

The present parametric analysis was performed with respect to the interspace, s, varied from $0.5mm$ to $2.5mm$, by fixing the other parameters of the SEHR circuit as shown in Table 1.

The obtained results for the s parametric analysis are plotted in Figure 9. We remind that the interspace, s, is linked to the coupling, k, between the transition lines TL and TL_D. We can understand from Figure 9(a) that the reflection coefficient is better when s is larger. However, the transmitted power, P_3, decreases when space is larger as illustrated in Figure 9(b). When changing the interspace, the transmitted energy, E_2, plotted in Figure 9(c) presents a negligible fluctuation. Finally, as seen in Figure 9(d), the amplitude of V_3 is inversely proportional to R_3 and decreases from $3.94V$ to $0.94V$ in the present range of value.

3.2.5. Parametric Analysis with Respect to w and w_d

In the present paragraph, the influence of TL widths, w and w_d is investigated by fixing the other electrical parameters and interspace, s, of the SEHR circuit as shown in Table 1. These widths were varied from $0.1mm$ to $7mm$ during the simulations.

Figure 10 presents the reflection coefficient simulated results of double parametric analysis for the widths w and w_d. It can be seen in Figure 10(a) and in Figure 10(b) that S_{11} and S_{22} change from about $-25dB$ to about $-3dB$. The best matching is located

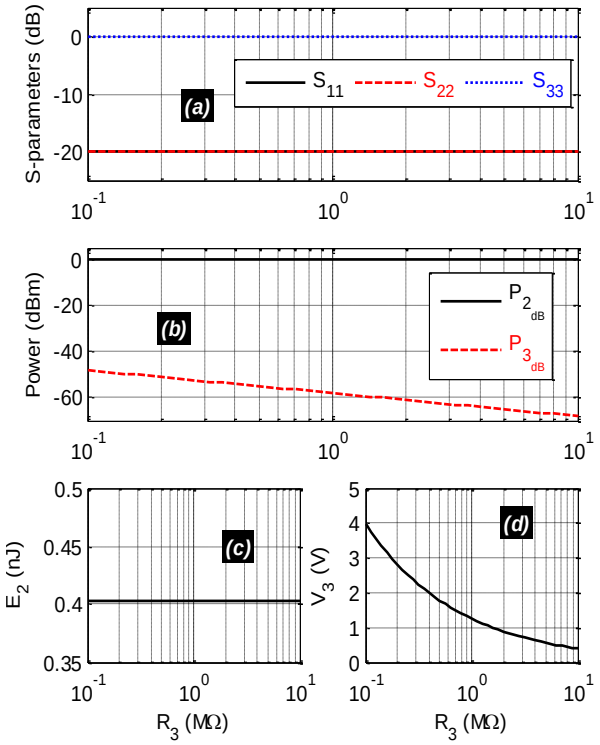

Figure 8.: Parametric analysis results with respect to R_3 (a) Reflection coefficients (b) Power (c) Energy per period, E_2 (d) Amplitude of voltage, V_3

for w between $2mm$ and $4mm$. The influence of w_d onto the reflection parameters is almost negligible. The S_{33} reflection coefficient remains very high in order of $0.1mdB$ in the considered range of widths.

The results of w and w_d parametric analyses with respect to the output powers, P_2 and P_3, are displayed in Figure 11. It can be seen in Figure 11(a), that P_2 is not sensitive to the variation of w_d. The best level of P_2 is reached when w is between $2mm$ and $4mm$. Figure 11(b) highlights that P_3 decreases when w_d increases. The maximal value of this power can be higher than $-10dBm$ for a w_d lower than $0.5mm$.

The influence of the TL widths on the transmitted average energy, E_2, is plotted in Figure 12(a). It can be seen that the maximal energy per period, of about $0.4nJ$, is reached for w between $2mm$ and $3mm$. The amplitude of transmitted signal voltage, V_3, in the function of (w, w_d) is mapped in Figure 12(b). The maximal voltage, evaluated of about $3.5V$, is located in the areahere the width couple is of about ($4.5mm$, $0.1mm$).

4. Conclusion

An original concept of SEHR is developed by using the CL structure. The topological analysis of the structure is introduced. The equivalent circuit based on the S-parameter approach is investigated. The influence of the unfamiliar loads connected to the SEHR is studied with parametric S-parameter simulations.

The influences of geometrical parameters as TL widths and interspace are also

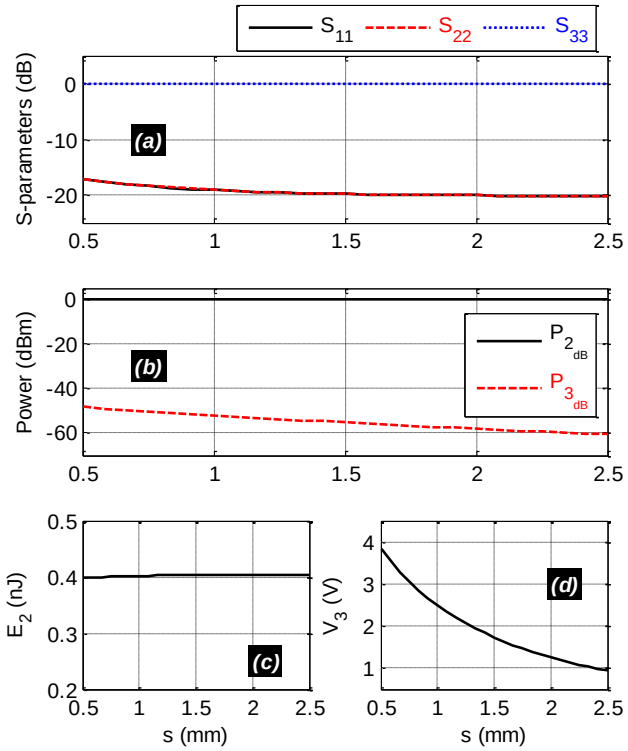

Figure 9.: Parametric analysis results with respect to s (a) Reflection coefficients (b) Power (c) Energy per period, E_2 (d) Amplitude of voltage, V_3

investigated. It enables to choose the optimal physical parameters to generate energy and also, signal voltage with significant amplitude. Otherwise, the choice of (w, R_2, R_3) plays a particular role to guarantee the matching between the data-signal transition and energy TL.

In a nutshell, the performed SEHR analysis and design can be helpful in the future to decide on the parametric trade-off according to the energy and data-signal loads depending on the given WSN-based mixed circuit technology EEs.

Overall, the performed SEHR analysis and design can be useful in the decision-making of the parametric trade-off following the energy and data-signal loads depending on the given WSN-based mixed circuit technology application.

References

[1] R. S. Sachan, R. Yadav and A. K. Rai, "A survey of energy-efficient communication protocols in WSNs," International Journal of Computer Engineering and Technology (IJCET), vol. 7, no. 3, May-June 2016, pp. 7–16.

[2] G. Anatasi, M. Conti, M. O. Francesco and A. Passarella, "Energy conservation in wireless sensor networks: A survey," Ad Hoc Networks, vol. 7, no. 3, May 2009, pp. 537-568.

[3] F. Pianegiani, M. Hu, A. Boni, and D. Petri, "Energy-Efficient Signal Classification in Ad hoc Wireless Sensor Networks," IEEE Transactions on Instrumentation and Measurement, vol. 57, no. 1, Jan. 2008, pp. 190-196.

[4] W. Sun, Z. Yang, X. Zhang, and Y. Liu, "Energy-Efficient Neighbor Discovery in Mobile Ad Hoc and Wireless Sensor Networks: A Survey," IEEE Communications Surveys and

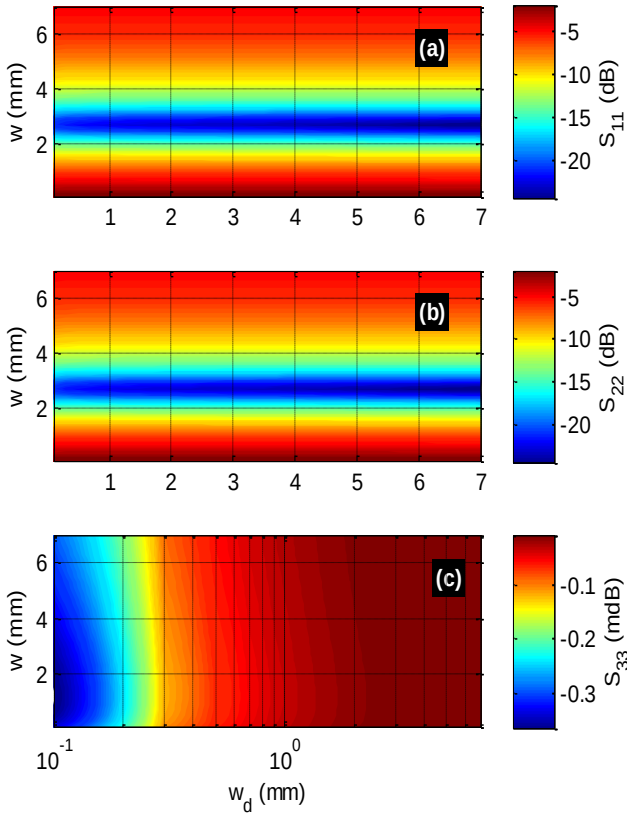

Figure 10.: Parametric analysis of reflection coefficients with respect to w and w_d (a) S_{11} (b) S_{22} (c) S_{33}

Tutorials, vol. 16, no. 3, 3rd quarter 2014, pp. 1448–1459.

[5] A. Devasena and B. Sowmya, "A study of power and energy efficient clustering protocols in wireless sensor networks," In. J. Adv. Research Computer Sci. Management Studies, vol. 1, no. 6, Nov. 2013, pp. 103-117.

[6] L.-O. Varga, G. Romaniello, M. Vucinic, M. Favre, A., Banciu, R. Guizzetti, C. Planat, P. Urard, M. Heusse, F. Rousseau, O. Alphand, E. Dublé, and A. Duda, "GreenNet: An Energy-Harvesting IP-Enabled Wireless Sensor Network," IEEE Internet of Things Journal, vol. 2, no. 5, Oct. 2015, pp. 412–426.

[7] D. C. Daly and A. P. Chandrakasan, "An Energy-Efficient OOK Transceiver for Wireless Sensor Networks," IEEE Journal of Solid-State Circuits, vol. 42, no. 5, May 2007, pp. 1003-1011.

[8] S. Sayilir, W.-F. Loke, J. Lee, H. Diamond, B. Epstein, D. L. Rhodes, and B. Jung, "A –90 dBm Sensitivity Wireless Transceiver Using VCO-PA-LNA-Switch-Modulator Co-Design for Low Power Insect-Based Wireless Sensor Networks," IEEE Journal of Solid-State Circuits, vol. 49, no. 4, Apr. 2014, pp. 996-1006.

[9] H.-M. Seo, Y. K. Moon, Y.-K. Park, D. Kim, D.-S. Kim, Y.-S. Lee, K.-H. Won, S.-D. Kim and P. Choi, "A Low Power Fully CMOS Integrated RF Transceiver IC for Wireless Sensor Networks," IEEE Trans. Very Large Scale Integration (VLSI) Systems, vol. 15, no. 2, Feb. 2007, pp. 227-231.

[10] C. Mahapatra, Z. Sheng, P. Kamalinejad, V. C. M. Leung and S. Mirabbasi, "Optimal Power Control in Green Wireless Sensor Networks With Wireless Energy Harvesting, Wake-Up Radio and Transmission Control," IEEE Access, vol. 5, Mar. 2017, pp. 501-518.

[11] A. D. Mauro and N. Dragoni, "On the Impact of Energy Harvesting on Wireless Sensor

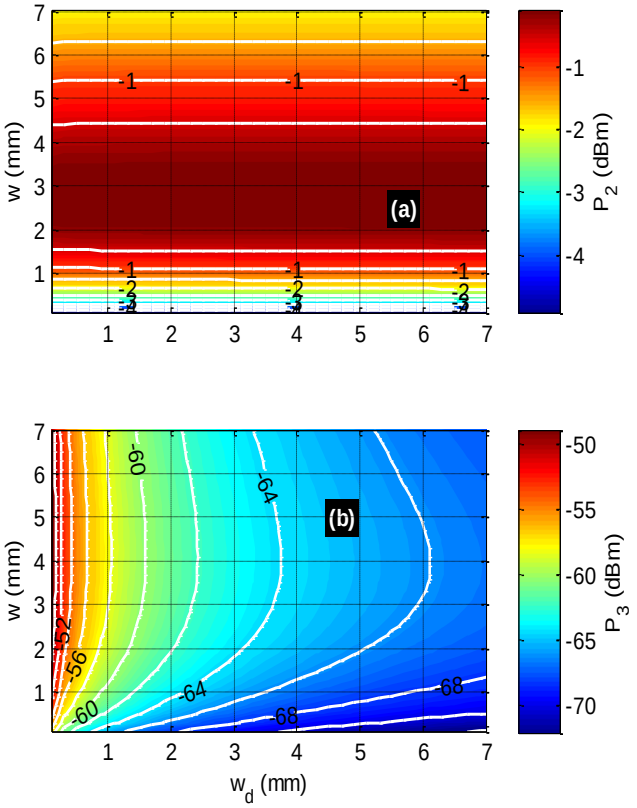

Figure 11.: Parametric analysis of average power with respect to w and w_d (a) P_2 (b) P_3

Network Security," PhD Thesis, Kgs. Lyngby: Technical University of Denmark (DTU), no. 349, 2015.

[12] S. Kosunalp, "A New Energy Prediction Algorithm for Energy-Harvesting Wireless Sensor Networks With Q-Learning," IEEE Access, vol. 4, Oct. 2016, pp. 5756-5763.

[13] J. M. Lebreton, "Systèmes et protocoles de télé-réveil appliqué à l'optimisation énergétique des réseaux de capteurs sans fil (in French)," PhD Thesis, Energy Lab, Univ. La Reunion, 197 pages, Avr. 2017.

[14] C. Wang, S. Guo, and Y. Yang, "An Optimization Framework for Mobile Data Collection in Energy-Harvesting Wireless Sensor Networks," IEEE Transactions on Mobile Computing, vol. 15, no. 12, Dec. 2016, pp. 2969–2986.

[15] J. C. Cowles, "The evolution of integrated RF power measurement and control," in Proc. of the 12th IEEE Mediterranean Electrotechnical Conference (IEEE Cat. No. 04CH37521), Dubrovnik, Croatia, 12-15 May 2004, pp. 131–134.

[16] D. Wang and X. Liao, "A novel symmetrical microwave power sensor based on GaAs monolithic microwave integrated circuit technology," Journal of Micromechanics and Microengineering, vol. 19, no. 12, pp. 125012.1-125012.8, Oct. 2009.

[17] Z. Zhang and X. Liao, "A lumped model with phase analysis for inline RF MEMS power sensor applications," Sensors and Actuators A: Physical, vol. 194, pp. 204-211, May 2013.

[18] R. P. Agarwal, R. C. Joshi Brajesh, K. Kaushik and S. Sarkar. "Crosstalk analysis and repeater insertion in crosstalk aware coupled vlsi interconnects," Microelectronics International, vol. 23, no. 3, pp. 55-63, 2006.

[19] S. Jiajun, R. Xiaoming, B. Liu, Z. Lixian and L. Shengchun, "Study on a New Combined Anti-Galloping Device for UHV Overhead Transmission Lines," IEEE Trans. Power

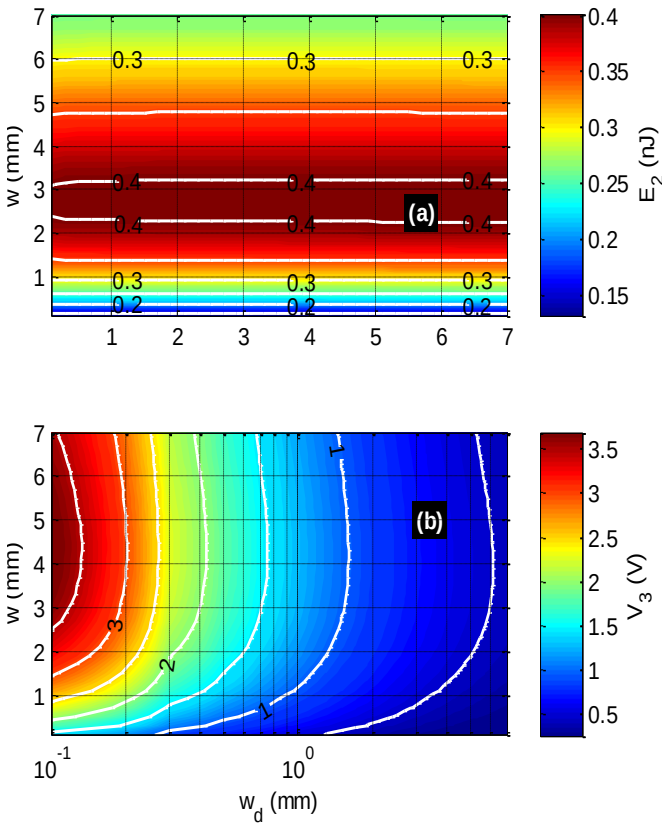

Figure 12.: Parametric analysis results with respect to w and w_d (a) Energy per period, E_2 (b) Amplitude of voltage, V_3

Delivery, 2019, pp. 1-1. 10.1109/TPWRD.2019.2911894.

[20] S. Luo, L. Zhu, and S. Sun, "Stopband-Expanded Low-Pass Filters Using Microstrip Coupled-Line Hairpin Units," IEEE Microwave and Wireless Components Letters, vol. 18, no. 8, Aug. 2008, pp. 506-508.

[21] A. Kosuge, S. Ishizuka, M. Taguchi, H. Ishikuroand T. Kuroda, "Analysis and design of an 8.5-469 Gb/s/link multi-drop bus using energy-equipartitioned transmission line couplers," IEEE Trans. CAS I: Regul. Papers, vol. 62, no. 8, pp. 2122–2131, Aug. 2015.

[22] B. Ravelo, L. Wu, F. Wan, W. Rahajandraibe and N. M. Murad, "Negative Group Delay Theory on li Topology," IEEE Access, Vol. 8, No. 1, Dec. 2020, pp. 47596-47606.

[23] B. Ravelo, "Theory on Coupled Line Coupler-Based Negative Group Delay Microwave Circuit," IEEE Trans. Microwave Theory Tech., vol. 64, no. 11, Nov. 2016, pp. 3604-3611.

[24] K. Kurokawa, "Power waves and the scattering matrix," IEEE Trans. Microwave Theory Tech., vol. 13, no. 2, Mar. 1965, pp. 194–202.

[25] H. Cho, D.E. Burk. A three-step method for the de-embedding of high frequency S-parameter measurements," IEEE Trans. Electron Devices, vol. 38, no. 6, pp. 1371-1375, June 1991.

[26] T. L. Moss and Y. Chen, "Mesh analysis for extracting the S-parameters of lumped element RF and microwave circuits," Int. Journal of Electrical Engineering Education, vol. 51, no. 4, pp. 330-339, Oct. 2014.

[27] R. Mita, G. Palumbo, and M. Poli, "Propagation Delay of an RC-Chain With a Ramp Input," IEEE Trans. CAS II: Express Briefs, vol. 54, no. 1, pp. 66-70, Jan. 2007.

[28] A. B. Kahng and S. Muddu, "An analytical delay model of RLC interconnects," IEEE Trans. Computer-Aided Design of Integrated Circuits and Systems, vol. 16, no. 12, pp.

1507-1514, Dec. 1997.
[29] R. Venkatesan, J. A. Davis and J. D. Meindl, “Compact distributed RLC interconnect models - part IV: unified models for time delay, crosstalk, and repeater insertion,” IEEE Trans. Electron Devices, vol. 50, no. 4, pp. 1094-1102, Apr. 2003.
[30] B. Ravelo, “Delay modelling of high-speed distributed interconnect for the signal integrity prediction,” Eur. Phys. J. Appl. Phys. (EPJAP), Vol. 57 (31002), Feb. 2012, pp. 1-8.
[31] S. Roy and A. Dounavis, “Efficient Delay and Crosstalk Modeling of RLC Interconnects Using Delay Algebraic Equations,” IEEE Trans. VLSI, vol. 19, no. 2, pp. 342-346, Feb. 2011.
[32] O. Maurice, A. Reineix, P. Durand, F. Dubois, ”Kron’s method and cell complexes for magnetomotive and electromotive forces,” Int. J. Applied Mathematics, Vol. 44, No. 4, pp. 183-191, 2014.
[33] M. Kirschning and R. H. Jansen, “Accurate Wide-Range Design Equations for the Frequency-Dependent Characteristic of Parallel Coupled Microstrip Lines,” IEEE Trans. Microwave Theory Tech., Vol. MTT-32, no. 1, pp. 83-90, Jan. 1984.
[34] A. Hammerstad and O. Jensen, “Accurate models for microstrip computer-aided design,” 1980 IEEE MTT-S International Microwave Symposium Digest, pp. 407-409, Washington, DC, USA, 28-30 May 1980.
[35] D. M. Pozar, “Microwave Engineering,” Wiley, 4th edition, NY, Nov. 2011.